PERGAMON

Journal of Structural Geology 25 (2003) 121–134

JOURNAL OF STRUCTURAL GEOLOGY

www.elsevier.com/locate/jsg

Ductile opening-mode fracture by pore growth and coalescence during combustion alteration of siliceous mudstone

Peter Eichhubl*, Atilla Aydin

Rock Fracture Project, Department of Geological and Environmental Sciences, Stanford University, Stanford, CA 94305-2115, USA

Received 14 September 2000; received in revised form 8 August 2001; accepted 20 September 2001

Abstract

Opening-mode fractures with blunt tips and large maximum apertures are characteristic of clinker that formed by combustion alteration of siliceous mudstone. These fractures are inferred to result from pore growth and coalescence, with initially circular pores inherited from the diatomaceous protolith. Circular pores grow preferentially in an en-échelon arrangement and coalesce to elongate pores and blunt-tipped fractures by thinning and rupture of bridges between pores. Coalescence of overlapping en-échelon pores causes fracture propagation in a zig-zag path that is considered indicative of significant inelastic deformation outside the immediate vicinity of the fracture tips. This process of fracture formation by void growth and coalescence is inferred to result from solution mass transfer and possible bulk melt movement during partial melting of clinker. Chemical mass transfer provides a mechanism for extensive inelastic deformation in the surrounding host rock concurrent with fracturing that is considered characteristic of ductile fracture. The preferred elongation of coalescing pores and local rupture of pore bridges is explained by a tensile sintering stress due to the thermodynamic tendency of the system for energy minimization of solid and liquid surfaces. It is suggested that ductile fracture processes that are accompanied by extensive inelastic deformation lead to opening-mode fractures with large apertures in a variety of crustal settings including metamorphic and magmatic systems as well as in reactive diagenetic environments, thus affecting fracture-controlled transfer of heat and mass and the rheology of the Earth's crust.

Keywords: Opening-mode fracture; Pore growth and coalescence; Siliceous mudstone; Clinker; Partial melting

1. Introduction

The understanding of brittle rock failure has progressed rapidly in recent years by applying principles of engineering fracture mechanics to rock testing, to numerical modeling of rock fracture, and to the structural interpretation of natural fracture systems (e.g. Ingraffea, 1987; Pollard and Segall, 1987; Pollard and Aydin, 1988; Engelder et al., 1993). Fracture mechanics regards fracture formation as the initiation and propagation of microcracks and their coalescence into macroscopic fractures. Crack propagation in rock is traditionally considered a brittle process of mechanical rupture of inter- and intra-granular bonds in a small process zone ahead of the crack tip (Whittaker et al., 1992). Outside the process zone, any strain associated with fracture opening and propagation is considered elastic. Fluid–mineral interaction may weaken bonds and assist in mechanical bond breakage (Atkinson, 1984). Despite this weakening effect, fracture propagation in environmentally assisted subcritical fracture is also considered a brittle process.

A different fracture process is known to occur in ductile metals and polymers at low temperatures as well as in ceramics at high homologous temperatures. In these materials, fracture propagation takes place by nucleation, growth, and coalescence of voids ahead of the fracture tip, typically preceded by tip blunting (Fig. 1) (Kinloch and Young, 1983; Evans and Blumenthal, 1984; Thomason, 1990; Wilkinson et al., 1991). In ductile metals, void growth and coalescence by the failure of ligaments between voids occur by crystal–plastic processes referred to as dislocation creep (Thomason, 1990). In ceramics at high homologous temperatures, void growth and coalescence may result from diffusion, solution, and dislocation creep, grain-boundary sliding, and viscous flow of an intergranular amorphous phase (Evans and Blumenthal, 1984; Wilkinson et al., 1991; Jin et al., 1999; Wiederhorn et al., 1999). In both types of materials, fracture opening is characterized by extensive inelastic deformation outside the immediate vicinity of the

* Corresponding author. Fax: +1-650-725-0979.
E-mail address: eichhubl@pangea.stanford.edu (P. Eichhubl).

0191-8141/02/$ - see front matter
PII: S0191-8141(02)00055-X

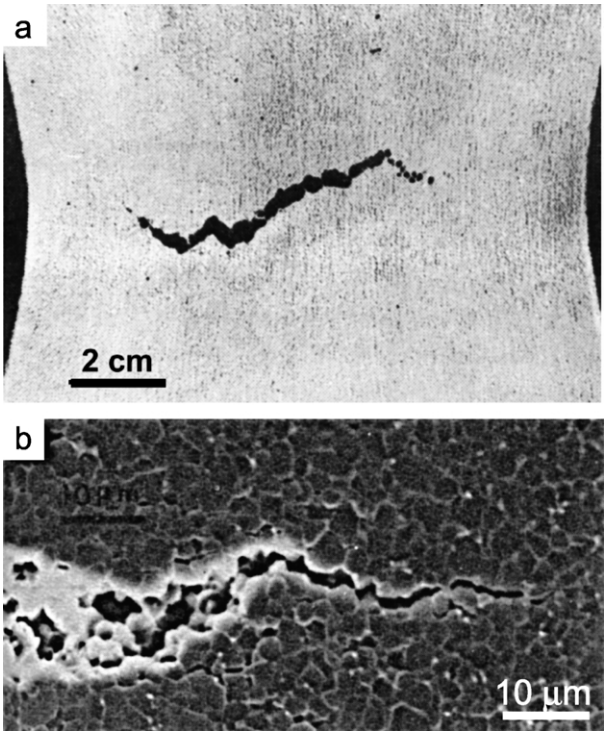

Fig. 1. (a) Ductile fracture in low-carbon steel formed in pure tension by nucleation, growth, and coalescence of pores (from Bluhm and Morrissey, 1965). (b) Ductile fracture in alumina at 1300 °C (from Dalgleish et al., 1984). Tension in both (a) and (b) applied in the vertical direction.

fracture tip and by large ratios of maximum fracture aperture over fracture length.

This study describes formation of opening-mode fractures by void growth and coalescence in siliceous mudstone that has undergone high-temperature/low-pressure alteration during natural in situ combustion of hydrocarbons. We shall demonstrate that fracture formation by void growth and coalescence in altered mudstone was accompanied by extensive inelastic deformation and textural reorganization associated with partial melting and formation of high-temperature minerals. It will be suggested that fracture processes observed in combustion-altered mudstone represent an end member case of ductile rock fracture that is characterized by large ratios of maximum aperture to fracture length and extensive deformation outside the immediate vicinity of the fracture tip. Although occurring under very specific temperature/pressure conditions, we believe that the fracture processes described here illustrate the potential coupling of fracture formation and mass transfer that is likely to be significant for both opening- and shearing-mode fracture in a variety of chemically reactive environments such as under metamorphic and magmatic conditions and in reactive diagenetic environments.

Following common usage in geologic and engineering fracture mechanics, the term ‘fracture’ designates two initially conjoined opposing surfaces that were separated by a displacement discontinuity, with end member modes of displacement being opening, shearing, and tearing. In this paper, we use ‘fracture’ for opening-mode fractures for simplicity, unless stated otherwise.

2. High-temperature alteration of siliceous mudstone at Orcutt Oil Field

At several localities in southern California, Miocene siliceous mudstone of the Monterey and Sisquoc Formations has undergone thermal alteration that has been attributed to in situ combustion of naturally seeping oil and gas (Bentor and Kastner, 1976). At Orcutt Oil Field south of Santa Maria, a quarry face provides a 40-m-high cross-section view across 3–4 subvertical, brecciated, 1–2-m-wide combustion centers and associated, partially overlapping alteration haloes that extend for up to 10–20 m into the surrounding formation (Cisowski and Fuller, 1987) (Fig. 2). These alteration zones are oriented at high angle to bedding, which strikes N80°E and dips 15° to NNW. Bedding is observed in unaltered mudstone as weakly developed preferred fissility that is obliterated in the altered rock units. Based on historic accounts of steam discharge from the ground at this location prior to quarrying (Arnold and Anderson, 1907), we infer that in situ combustion occurred in recent geologic times under near-surface conditions.

We defined and mapped six distinct alteration zones based on macroscopic criteria such as rock color and hardness. From least to most altered, these are: unaltered siliceous mudstone, coked mudstone, oxidized and bleached oxidized mudstone, sintered oxidized mudstone, and clinker (Fig. 2; unaltered and coked mudstone and oxidized and bleached oxidized mudstone were not differentiated for rock physical analyses given in Eichhubl et al. (2001)). Unaltered siliceous mudstone is friable and dark-gray to bleached-white in color. Coked mudstone is black to dark gray, with a gradational transition to unaltered mudstone and a sharp front facing bleached oxidized mudstone. Oxidized and bleached oxidized mudstones are similar to unaltered mudstone in friability but distinct by a uniform to spotty brick-red to orange color. A subtle but distinct increase in induration marks the sharp outer boundary of sintered oxidized mudstone. Over a narrow, 1–3-cm-wide transition zone, sintered oxidized mudstone changes to clinker, which is similar in hardness to fired clay brick and dark red and purple to black in color.

2.1. Methods

Samples for thin sectioning, XRD, XRF, and microprobe analyses were taken along two bedding-parallel traverses across alteration zone boundaries, one traverse along the base and another along the second terrace of the quarry (letters C to L in Fig. 2). Two additional samples (A and B) of unaltered mudstone were taken 200–300 m away from the quarry from stratigraphic horizons roughly equivalent to those sampled in the quarry. Samples for thin-section and

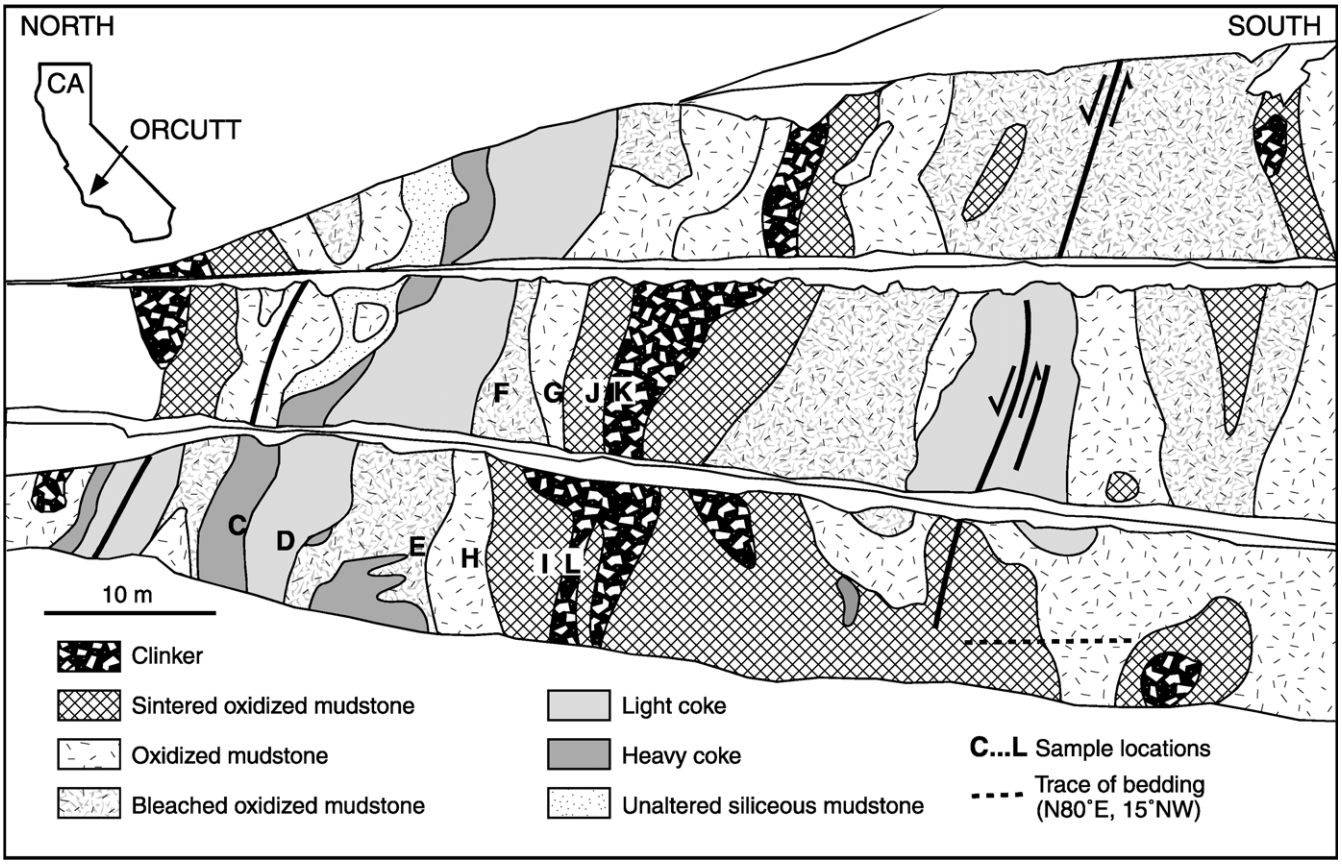

Fig. 2. Outcrop map of the northern half of a stepped quarry face in Orcutt Oil Field that provides a cross-section view of alteration haloes around centers of natural combustion. Alteration zones were defined in the field based on macroscopic criteria such as rock color and hardness.

microprobe analyses were vacuum impregnated with blue-dyed epoxy prior to thin sectioning. Blue epoxy impregnation allowed recognition of potential deformation artifacts that may have resulted from sample preparation and thin sectioning. Samples for semi-quantitative XRD analysis were ground in an agate mortar and mixed with 17%$_{weight}$ corundum as internal standard. Both oriented and random powder mounts were measured over 4–55° 2θ with 0.02° stepping angle and a 6 s count time on a Rigaku X-ray diffractometer at Stanford University. Mineral peaks used for semi-quantitative estimates of mineral abundance are listed in Table 1. Bulk rock samples were analyzed by XRF at the GeoAnalytical Laboratory at Washington State University following procedures described by Johnson et al. (1999).

Table 1
XRD peaks used for semi-quantitative estimates of mineral abundance in altered siliceous mudstone

	hkl	°2θCuKα	Intensity
Quartz	100	20.8	22
	101	26.6	100
Cristobalite	101	21.9	100
Tridymite	112	20.5	90
Opal-A	–	~21.8	100
Plagioclase	−204	27.9	100
Cordierite	132	26.3	70
	151	29.3	65
Hematite	104	33.1	100
Montmorillonite	001	5.8	100
Illite	002	8.8	35
Kaolonite	001	12.3	100
Corundum[a]	012	22.5	75
	104	35.1	90

[a] Added as internal standard.

2.2. Compositional and textural changes during combustion

Unaltered siliceous mudstone consists of biogenic opal-A and smectite as main constituents, with minor opal-CT, kaolinite, illite, quartz, and feldspar (Fig. 3). The stability of opal-A and beginning occurrence of opal-CT indicates temperatures of 40–50 °C (Keller and Isaacs, 1985) during regional burial diagenesis of the formation prior to exhumation and combustion alteration. Coked mudstone is indistinguishable from unaltered siliceous mudstone in mineralogical composition. Oxidized mudstone as well as bleached oxidized mudstone are characterized by the beginning instability of smectite–montmorillonite and the formation of hematite. In sintered oxidized mudstone, cristobalite precipitates at the expense of opal-A. Clinker is characterized by the instability of illite and beginning instability of quartz, and by the formation of tridymite,

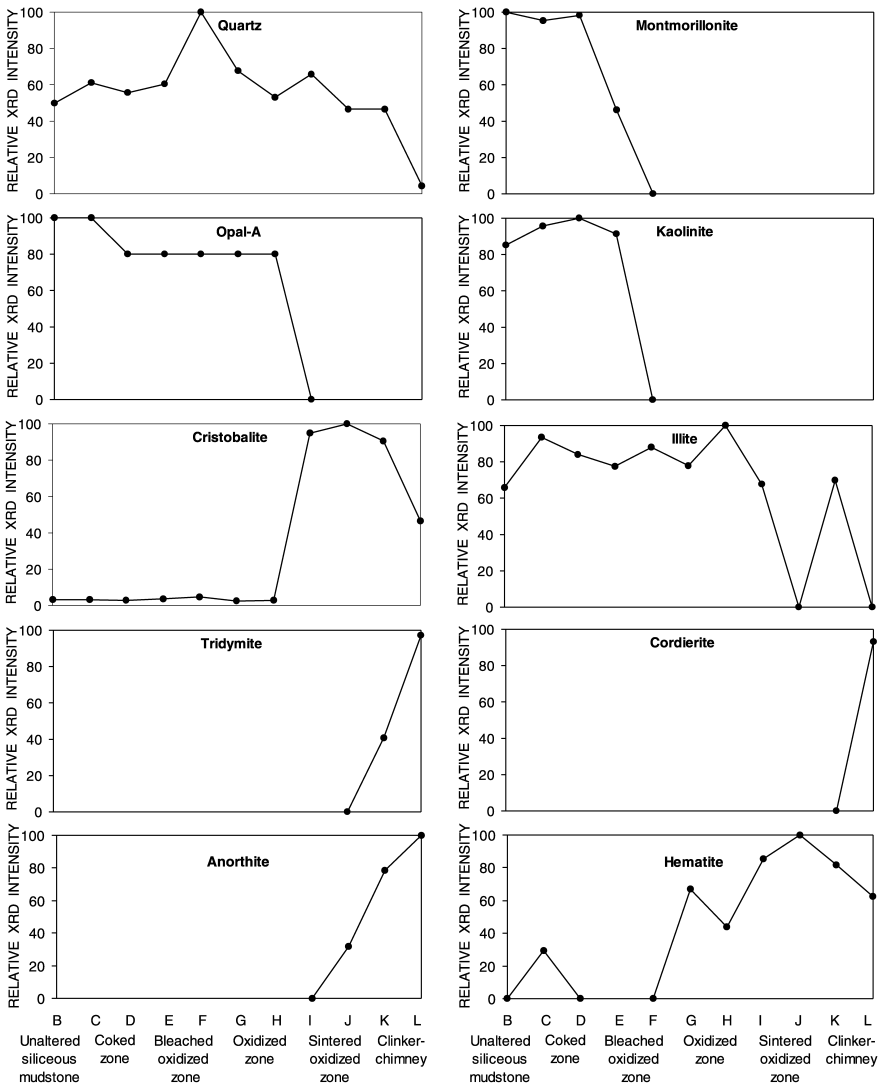

Fig. 3. Profiles of mineral abundance across alteration zones based on semi-quantitative XRD analysis. See Fig. 2 for sampling locations of samples C–L; sample B of unaltered mudstone was taken outside the quarry. Peaks and peak hights used for analysis are listed in Table 1.

cordierite, and calcic plagioclase (anorthite component An 0.6–0.7).

The texture of partially fused and interlocking diatoms as seen in ultra-thin sections of unaltered siliceous mudstone (Fig. 4a) is still well preserved in oxidized mudstone (Fig. 4b), with the addition of finely dispersed hematite. In sintered oxidized mudstone (Fig. 4c), opal-A dissolution leaves molds of diatom tests while cristobalite precipitates in the surrounding matrix. Hematite occurs in clusters. A complete microstructural rearrangement accompanies the transition from sintered oxidized mudstone to clinker (Fig. 4d). Grains of detrital quartz and corroded plagioclase are contained in a matrix of finely intergrown plagioclase, tridymite, and cordierite (Fig. 5). The intergrowth of plagioclase and tridymite has a crystallographic regularity resembling a micrographic texture, consisting of a 1–2-μm-thick latticework of plagioclase and interstitial tridymite (Fig. 5b) suggesting eutectic co-precipitation of both phases from a melt phase. Cordierite crystals of typically <5 μm diameter are suspended in the plagioclase latticework. Hematite re-precipitated as 10–20-μm-long laths, forming radial arrangements adjacent to the surface of pores (Fig. 6). Detrital grains of plagioclase have a rim that is enriched in Ca (An 0.6–0.7) relative to the core (An 0.6), with the contact between rim and core sharp and irregularly embayed. Based on a comparison with a similar texture produced in melting experiments by Johannes (1989), this rim is interpreted as a melt corrosion margin, suggesting the presence of an intergranular melt phase (Eichhubl et al., 2001). No evidence of glass, although common at other locations of natural combustion alteration of siliceous mudstone (Bentor and Kastner, 1976; Bentor et al., 1981), is observed in XRD or thin section.

Despite the formation of microscopic pores at the transition from sintered oxidized mudstone to clinker (Fig. 4), Eichhubl et al. (2001) reported an overall decrease in porosity from an initial 62% in unaltered mudstone to 47% in sintered oxidized mudstone and 28% in clinker. This

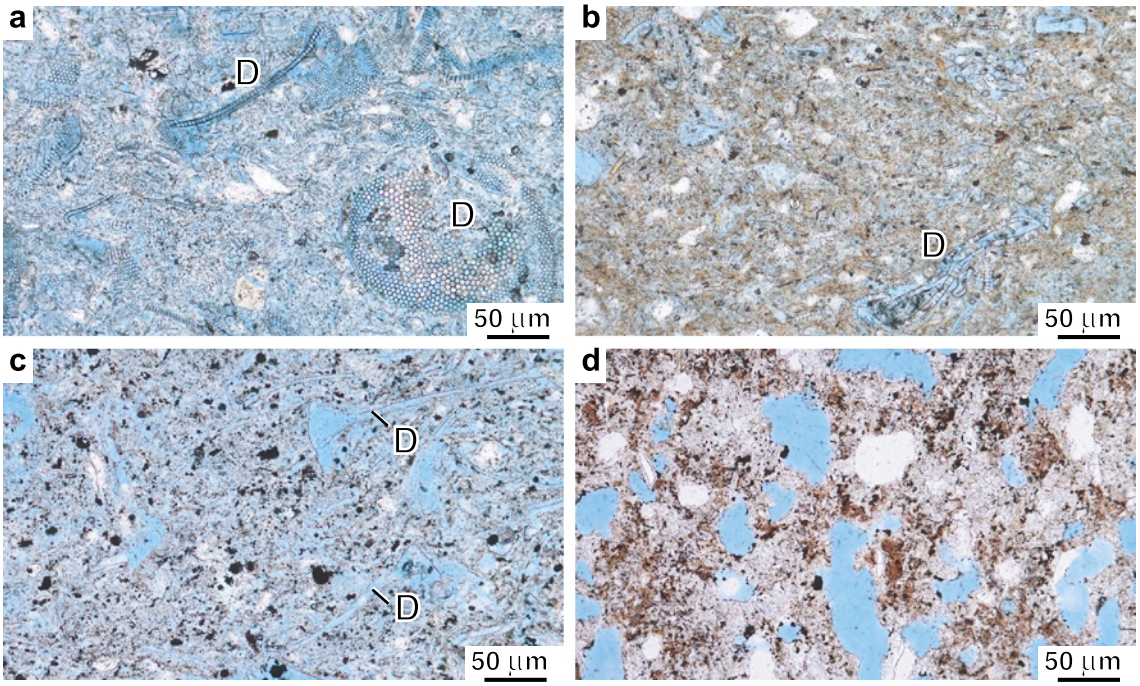

Fig. 4. Photo-micrographs of alteration sequence in siliceous mudstone at Orcutt oil field. (a) Unaltered siliceous mudstone with partially dissolved and fused diatom tests (D). (b) Oxidized siliceous mudstone, in composition similar to (a) but with addition of finely dispersed hematite. (c) Sintered oxidized mudstone with molds of dissolved diatom tests (D). (d) Clinker. Notice change in pore geometry that is most pronounced between sintered oxidized mudstone and clinker. Some unconnected pores in clinker remained unfilled during blue-epoxy impregnation and are now filled by white mounting epoxy.

reduction in porosity indicates a loss in sub-microscopic porosity in siliceous mudstone.

XRF bulk rock analyses across alteration zones (Fig. 7), from unaltered siliceous mudstone to clinker, indicate no significant changes in Si and Al concentrations. Total $Fe^{(2+,3+)}$, expressed in Fig. 7 as FeO, shows a slight, but steady, increase towards the alteration center. Concentrations of Na, K, and Ca drop in the sintered oxidized zone and increase again in the clinker, in part exceeding concentrations outside the combustion zone. Mg and Mn are similarly depleted in the alteration halo, including the oxidized zone.

3. Blunt-tipped fractures

Clinker and, to a lesser extent, sintered oxidized mudstone are characterized by the occurrence of blunt-tipped opening-mode fractures, i.e. fractures with no discernible shear displacement (Fig. 8). In sintered oxidized mudstone and in the outer parts of clinker, these fractures are isolated or occur in en-échelon arrays and are increasingly connected toward the central part of clinker forming a breccia. Unlike systematic joints in unaltered siliceous mudstone outside combustion zones, these fractures are characterized by high aspect ratios of maximum aperture over length that exceeds 1:50 for macroscopic fractures longer than 1 mm, and 1:10 for microscopic fractures shorter than 1 mm (Fig. 9). The shape of macroscopic fractures is characterized by a concave taper to blunt tips. While the orientation of blunt-tipped fractures within a combustion center is uniformly distributed (Lore et al., 2002), neighboring fractures preferentially intersect at high angles that approach 90° (Fig. 8a). The surface of blunt-tipped fractures is macroscopically rough with no distinct hackle marks or arrest lines. Hairline fractures may originate at blunt fracture tips. Whereas blunt-tipped fractures are spatially associated with increased alteration as describe further below, hairline fractures lack such association and are thus interpreted to form after combustion.

The largest blunt-tipped fractures are up to 5 cm long and 5 mm in aperture. A continuous size distribution is observed from macroscopic blunt-tipped fractures to elongate pores <1 mm in length and to circular pores <100 μm in diameter (Figs. 8–10). Elongate pores occur preferentially at the tips of larger elongate pores or of blunt-tipped fractures in a left or right stepping en-échelon array (Fig. 10). A zig-zag alignment of pores of about 45° around their mean long axis reflects the alternating preference in stepping direction (Figs. 8b and 10). Within these arrays, pores become larger and remaining bridges between pores thinner toward the tips of blunt-tipped fractures. A progression of bridge thinning and concomitant pore growth apparently leads to coalescence of neighboring pores within an array. Bridge thinning occurs preferentially between elongate

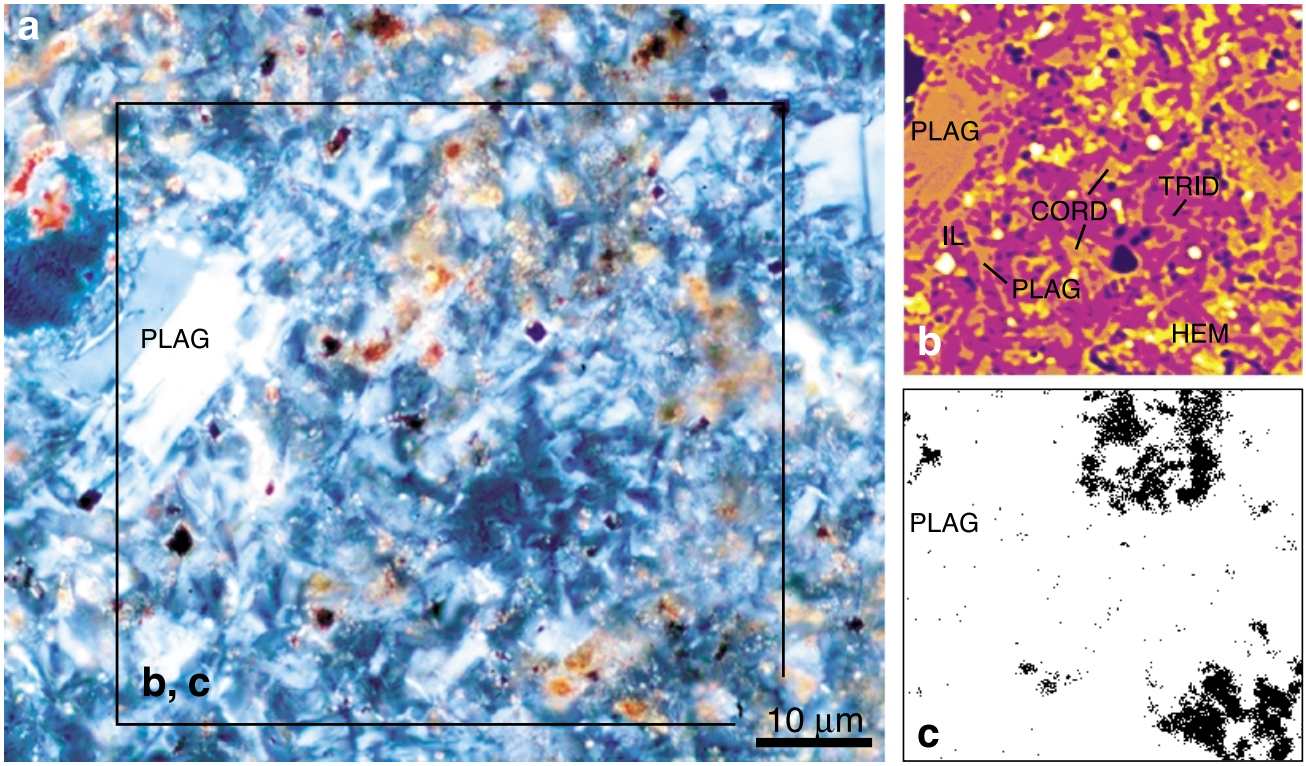

Fig. 5. Cross-polarized light photomicrograph (a), backscatter image (b), and potassium map (c) of clinker, composed of a latticework of plagioclase (laths of purple color in (b)) and interstitial tridymite (blue in (b)). Other phases are cordierite, hematite, ilmenite, and detrital grains of plagioclase (left). Blue-purple colors are phases of low mass number, orange-yellow colors correspond to high mass number. PLAG: plagioclase, CORD: cordierite, TRID: tridymite, HEM: hematite, IL: ilmenite.

pores that are aligned en échelon and partially overlap (Fig. 11a) and less frequently between pores in a tip-to-tip arrangement (Fig. 11c).

In addition to increased pore growth toward the tip of larger elongate pores and blunt-tipped fractures, an increased density of smaller fractures and pores is found along the sides of larger fractures (Fig. 12). This increased fracture and pore density appears to correlate with an increased alteration of clinker adjacent to larger fractures. Similar to pores at fracture tips, pores adjacent to the sides of larger fractures display a progression of bridge thinning and coalescence with these larger fractures.

Pores along sides of fractures appear to coalesce by ultimate thinning of bridges between pores and fracture space (Fig. 11d). In contrast, bridges between elongate pores that are in an en-échelon or tip-to-tip arrangement are observed to fail by a combination of bridge thinning and ultimate bridge rupture (Fig. 11c). In both cases, failed bridges develop into blunt protrusions of fracture walls into the fracture space (Fig. 11b). The irregularity of pitted fracture walls due to surface embayments and protrusions (Fig. 10a) reflects the coalescence of pores and the blunting of bridge remnants following bridge thinning and rupture.

4. Discussion

4.1. Ductile fracture by pore growth and coalescence in comparison with brittle fracture propagation

The progressive stages of pore growth and bridge failure in the vicinity of fractures indicate that blunt-tipped fractures form by growth and coalescence of elongate pores with coalescence taking place by thinning of bridges between pores and ultimate bridge rupture. The preferred growth and coalescence of pores in the tip region of fractures leads to an increase in fracture length whereas slower growth and coalescence of pores adjacent to fracture surfaces causes a proportionally smaller increase in fracture aperture. Preferred lengthening of pores over widening explains the decrease in aspect ratio from microscopic pores to macroscopic blunt-tipped fractures (Fig. 9). Whereas pores grow preferentially within two arrays ahead of fracture tips at directions that form a 30 to 45° angle with respect to the fracture long axis, the alternation between left and right stepping arrays leads to a macroscopic fracture propagation direction that coincides with the mean long-axis direction of elongate pores and fractures.

Conventional brittle fracture of rock involves fracture nucleation and propagation due to stress concentration at the crack tip and resulting mechanical rupture of inter- and

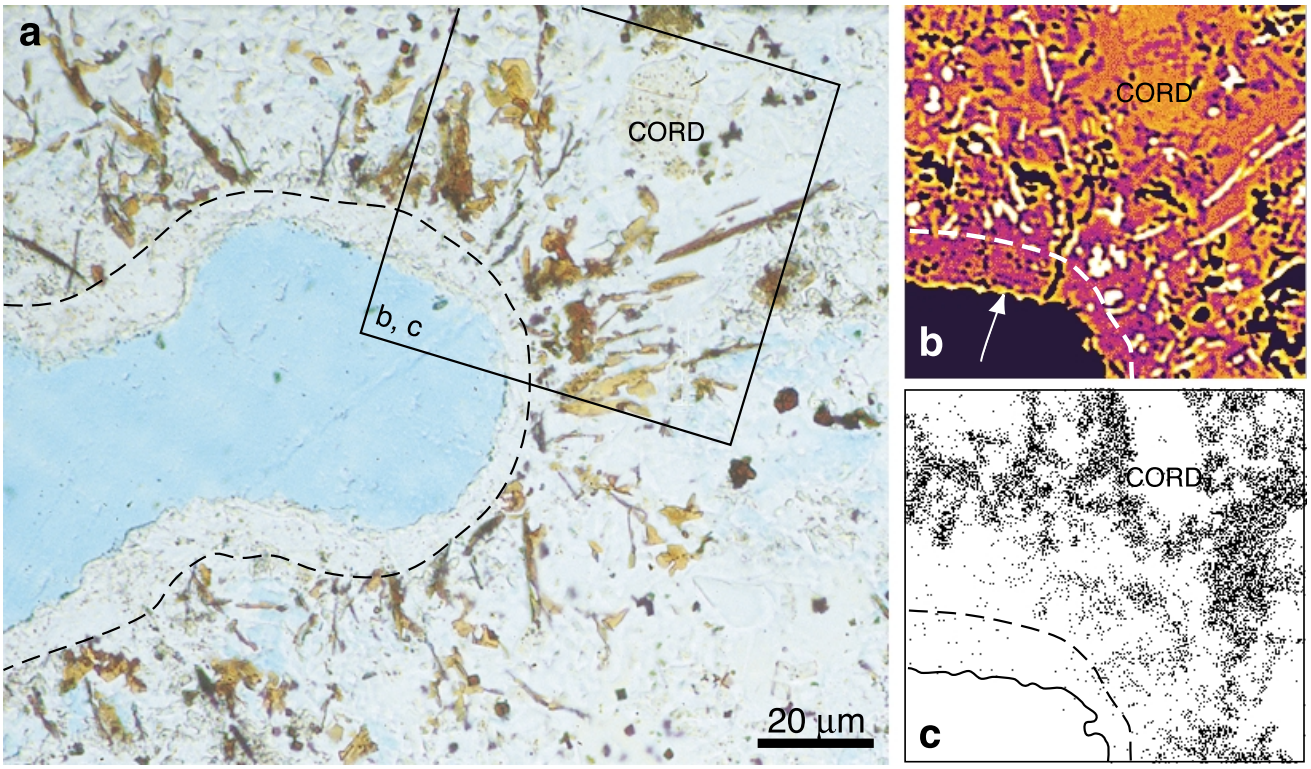

Fig. 6. Plain-polarized light photomicrograph (a), backscatter image (b), and potassium map (c) of clinker. Pore, impregnated with blue epoxy, is surrounded by a quartz-rich rim (dashed in (a)) that is enriched in aluminum along the outer margin (arrow in (b)). Laths of hematite radiate away from the pore. CORD: cordierite.

intra-granular bonds. Bond breakage produces micro-flaws within a process zone that extends from the crack tip over a short distance into the rock. Growth and coalescence of flaws within the process zone leads to fracture propagation. The size of the process zone is limited as the fracture tip stress concentration drops with $1/\sqrt{r}$ away from the fracture tip resulting in sharp fracture tips. In sandstone, a fully developed process zone may be 1–3 mm in radius (Peck et al., 1985). Because the highest flaw density is, in an otherwise homogeneous material, concentrated at the fracture tip, brittle opening-mode fractures propagate from the fracture tip outward following a straight or curvilinear path that is perpendicular to the local least principal stress at the fracture tip.

In contrast to brittle rock fractures, fracture formation in clinker is characterized by: (1) growth and coalescence of circular to elliptical pores rather than thin micro-flaws; (2) blunt fracture tips; (3) pore growth in 30–45° en-échelon arrays leading to zig-zag fracture propagation paths; and (4) pore growth outside the immediate vicinity of the fracture tip. Points (1) through (3) and, to some extent, point (4), are common to fracture processes in ductile metals and in ceramics at high homologous temperatures (Fig. 1) (Evans and Blumenthal, 1984; Thomason, 1990; Wilkinson et al., 1991; Wiederhorn et al., 1999). In these materials, plastic or viscous flow associated with tip blunting induces preferred void nucleation and growth along two 30–45° axes ahead of the crack tip. Voids coalesce by thinning and rupture of bridges between voids. Coalescence of voids may switch between the two 30–45° axes causing fracture propagation along a zig-zag path similar to that seen in clinker (Fig. 1). In ductile metals, fracture growth by void coalescence produces characteristic dimpled fracture surfaces with sharp-tipped torn ligaments.

Following Thomason (1990), the zig-zag path of ductile fracture propagation results from preferred void growth and coalescence along characteristic directions in a plastic velocity field. Within the framework of plasticity theory, characteristics are surfaces along which normal and tangential strain rate tensor components lying in these surfaces are zero and other strain rate components are undetermined (Hill, 1950). Regarding ductile fractures as velocity discontinuities, Thomason (1990) suggested that void growth and coalescence occurs preferentially along characteristic directions along which stationary velocity discontinuities of non-zero normal and tangential components with respect to these surfaces can develop in an initially continuous velocity field while maintaining geometric compatibility. In a plain-strain plastic velocity field, these characteristic surfaces coincide with surfaces of maximum shear strain rate at 45° to the direction of maximum shortening rate. In a axisymmetric strain-rate field, this angle decreases to 35°.

The 30–45° orientation of preferred void coalescence direction and the resulting zig-zag fracture propagation path may thus be considered indicative of significant inelastic

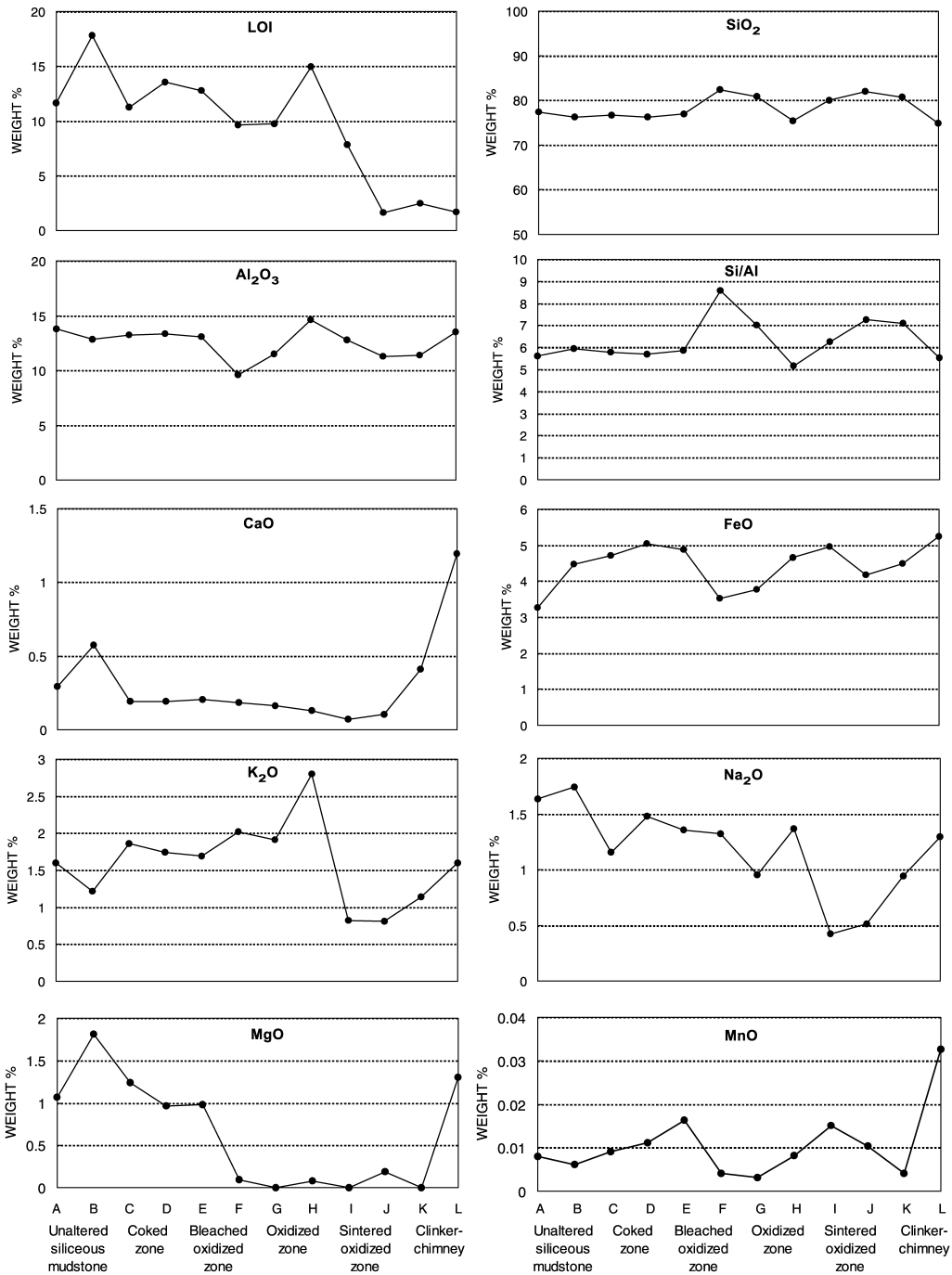

Fig. 7. Profiles of loss on ignition (LOI) and elemental composition across alteration zones based on XRF bulk rock analyses. XRF values are normalized to a volatile-free basis with Fe total expressed as FeO. LOI analyses by ignition to 900 °C over 3 h. Samples B–L are same as in Fig. 3. Sample A of unaltered mudstone was taken outside the quarry.

deformation outside the immediate vicinity of the fracture tip and characteristic of ductile opening-mode fracture. Such a zig-zag propagation path is not expected for brittle fracture where inelastic deformation is restricted to a small process zone at the fracture tip. Elastic interaction among brittle opening-mode fractures that are arranged in en-échelon arrays may allow coalescence to a through-going fracture system that is oriented oblique to the least principal far-field stress (Nicholson and Pollard, 1985; Du and Aydin, 1991; Olson and Pollard, 1991). However, the process of coalescence associated with brittle fracture is different from that of ductile fracture. Brittle fractures coalesce in en-échelon arrays by curving and propagating toward each other and/or by bending of bridges between overlapping en-échelon fractures (Fig. 13) (Nicholson and Pollard, 1985; Olson and Pollard, 1991). Both processes are not observed in clinker where elongate pores in en-échelon arrays coalesce by thinning of bridges between overlapping

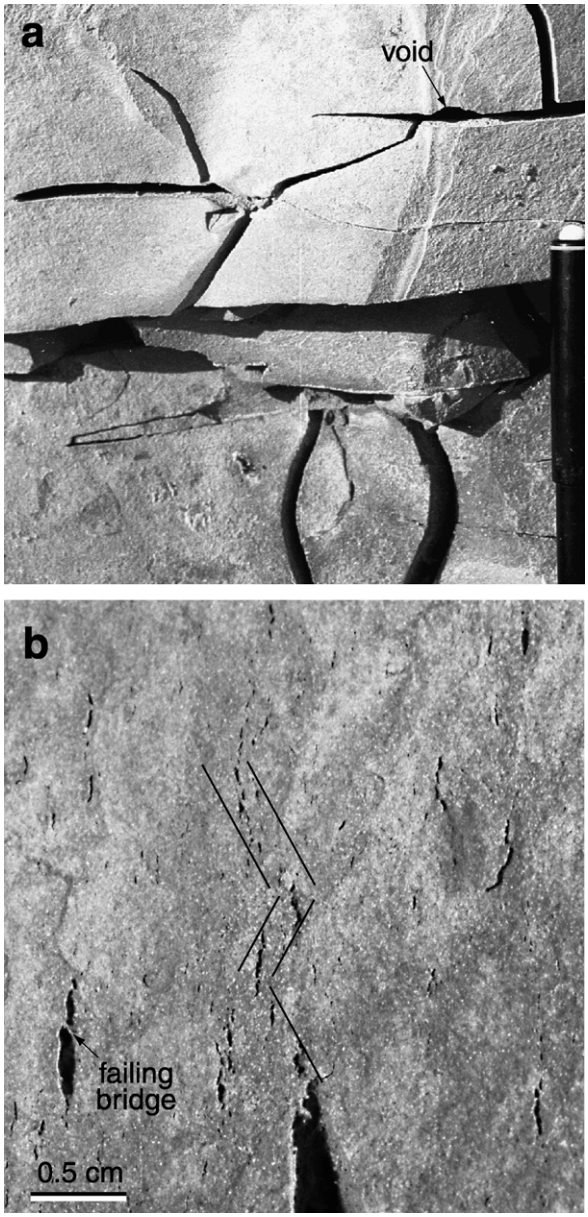

Fig. 8. Blunt-tipped opening-mode fractures in clinker. (a) Opening-mode fractures in clinker are characterized by blunt tips and high intersection angles that approach 90°. Pen for scale. (b) Close-up view of a fracture tip. Notice en-échelon arrays of fractures and failing bridges within these arrays.

elongate pores. Elastic interaction has also been shown to favor fracture propagation in uniform, either left or right-stepping, arrays (Du and Aydin, 1991) rather than alternating between left- and right-stepping arrays as observed as zig-zag propagation paths in clinker, ductile metals, and ceramics at high temperatures.

4.2. Pore coalescence and mass transfer

Unlike fracture in ductile metals and ceramics at high-temperatures where pore nucleation or cavitation precedes pore growth, pore growth in clinker is inferred to take

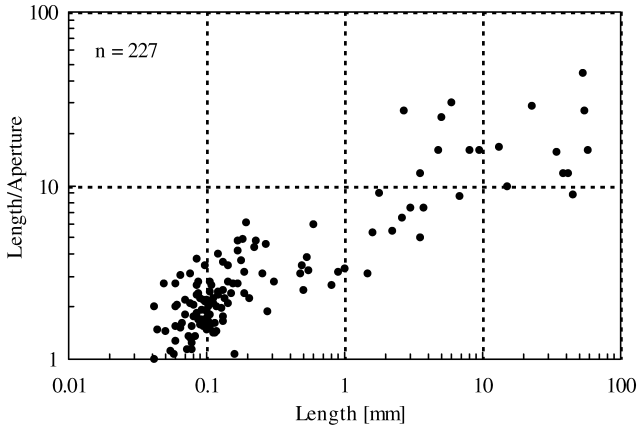

Fig. 9. Ratio of fracture length over aperture plotted versus fracture length of blunt-tipped opening-mode fractures in clinker.

advantage of pores that already exist in sintered oxidized mudstone. Dissolution of opal-A in sintered oxidized mudstone produces molds after diatom tests as large as 50 μm across (Fig. 4c). The formation of unfilled molds involves silica transport away from diatom tests, presumably filling sub-micron matrix porosity that is inherited from the diatomaceous protolith. Continued pore growth in clinker requires additional mass transport away from pore walls. The effect of mass transfer on a grain scale (< 1 μm) is observed through the formation of the plagioclase–cordierite–silica lattice of clinker (Fig. 5b) requiring transport and structured rearrangement of ions. Mass transfer on a transgranular scale of 1–10 μm can be inferred based on the dissolution of finely dispersed hematite in sintered oxidized mudstone and the re-precipitation of hematite as up to 10-μm-long laths around pores in clinker (Fig. 6). These laths form radiating arrays around pores, indicative of hematite re-precipitation involved in the growth of pores by diffusive mass transfer. We infer that mass transfer required for the growth and coalescence of pores was accomplished by mineral dissolution in the partial melt phase and by diffusive mass transport of ions in the melt phase. The presence of a partial melt phase in clinker during combustion alteration is indicated by the zoned and corroded nature of detrital grains of plagioclase (Eichhubl et al., 2001), the eutectic intergrowth texture of plagioclase and tridymite (Fig. 5b), and the compositional zoning of some pore walls (Fig. 6a–c). Zoned pore walls are composed of an outer silica and inner aluminum enriched rim (Fig. 6b) that may have formed by the crystallization of melt along pore walls. Pore linings as shown in Fig. 6 are only locally developed in clinker, which may be indicative of bulk movement of melt. Mass transfer on a 1-m-scale associated with combustion alteration is indicated by increased Ca, Mg, Mn, Na, and K concentrations in clinker compared with adjacent sintered oxidized mudstone (Fig. 7).

The formation of larger pores in clinker, accompanied by an overall decrease in porosity (Eichhubl et al., 2001), indicates growth of larger pores at the expense of smaller

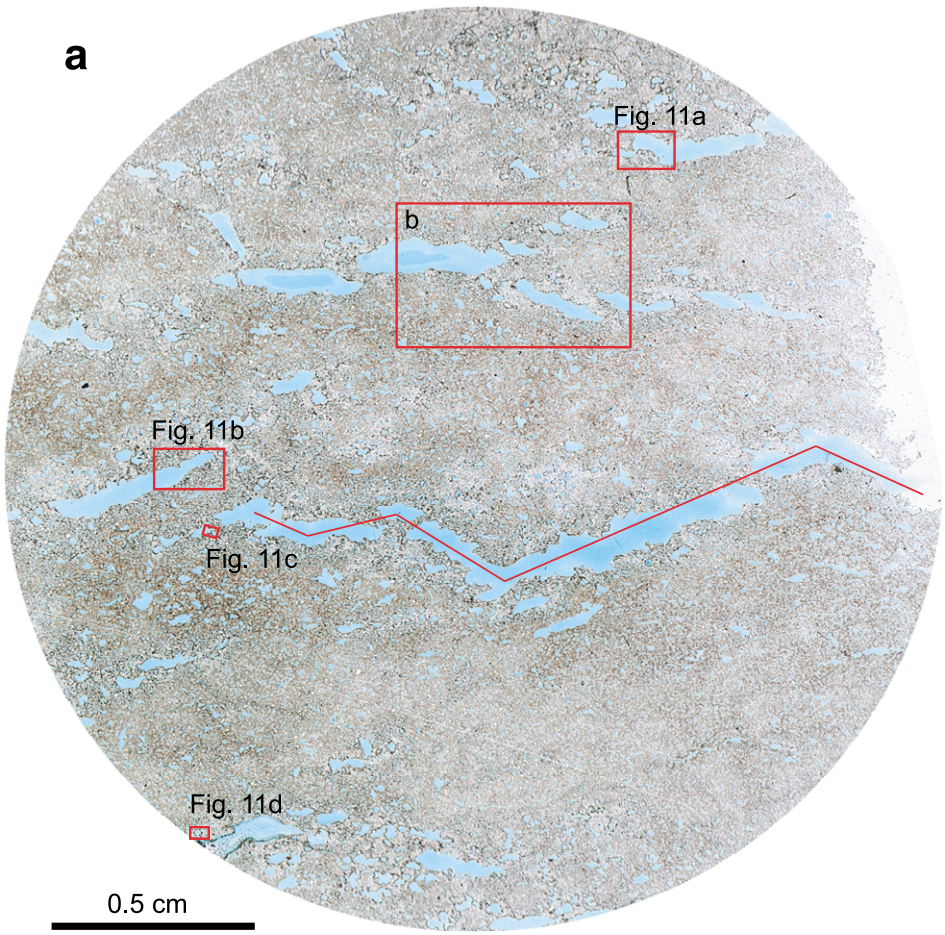

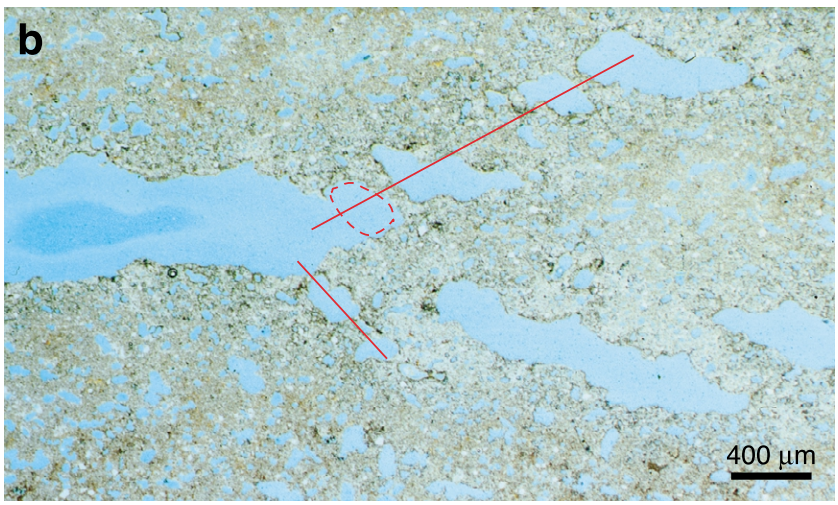

Fig. 10. (a) Photo-micrograph of core plug in clinker illustrating the transition from elongate pores to macroscopic blunt-tipped fractures. Zig-zag fracture path is outlined. (b) Fracture tip with arrays of elongate pores in the tip region and different stages of pore coalescence by bridge failure. Dashed line indicates shape of pore that had coalesced with the main fracture in an earlier stage.

ones. Preferred pore growth and coalescence is observed adjacent to macroscopic fractures (Fig. 12) suggesting a positive feedback between alteration and fracture formation. Such a feedback could be due to enhanced advective heat transfer within fractures.

Continued pore growth by diffusive mass transfer leads to bridge thinning and eventual pore coalescence. Diffusive mass transfer also results in rounding and eventual removal of remaining parts of failed bridges (Fig. 11b). While diffusive mass transfer appears to be the predominant

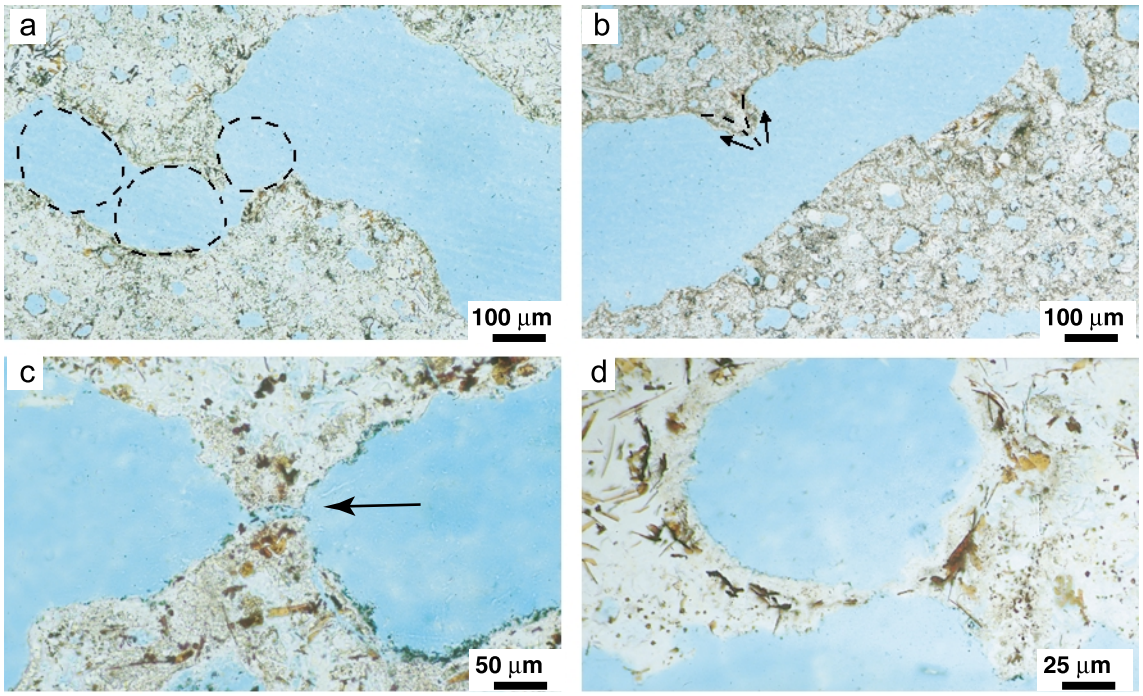

Fig. 11. Modes of bridge failure between adjacent pores (details of Fig. 9a). (a) Failed bridge between two en-échelon arranged elongate pores. (b) Rounded remnant of failed bridge is indicative of mass transfer away from the tip of the failed bridge. (c) Ruptured bridge from the tip region of a larger elongate pore. The presence of blue impregnation epoxy, rather than white mounting epoxy, within the ruptured bridge (arrow) indicates that bridge rupture is not an artifact of thin section preparation because blue-epoxy vacuum impregnation was performed before thin section preparation. (d) Pore adjacent to a larger elongate pore is about to coalesce by ultimate bridge thinning without rupture.

mechanism of pore growth and coalescence, rupture of some bridges (Fig. 11c) is indicative of a tensile stress. A deviatoric tensile stress is needed to explain the formation of elongate rather than circular pores.

4.3. Driving forces involved in ductile fracture

Whereas void growth and coalescence in metals is typically confined to a plastic zone ahead of the fracture tip of radius $2d$ where d is the crack-tip opening displacement

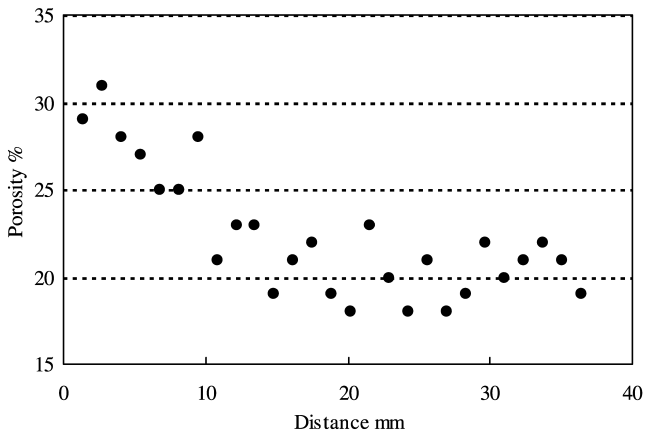

Fig. 12. Porosity profile away from a macroscopic large-aperture fracture in clinker. Porosity was determined by image analysis of a blue-epoxy impregnated thin-section along a 3 mm wide sampling traverse perpendicular to the macroscopic fracture surface, using 1.3 mm sampling intervals.

(Anderson, 1995), void growth and coalescence in clinker occurs well beyond this distance. This difference in the extent of damage associated with fracture between clinker and ductile metals is likely to reflect differences in loading conditions. Under typical fracture resistance tests of metals and ceramics, void nucleation, growth, and coalescence result from tensile mechanical loading imposed from outside the system. Based on a comparison of porosity reduction at the transition from sintered oxidized mudstone to clinker with the fracture strain measured in clinker, Eichhubl et al. (2001) inferred that the strain accommodated by opening-mode fracturing of clinker was compensated by porosity reduction and not the result of net extension of the clinker zone. Without net extension, pore growth and resulting formation of blunt-tipped fractures was inferred to result from tensile stresses associated with partial melting, reaction between melt and remaining solids, and melt redistribution. The formation of tensile stresses associated with grain-scale mass transfer and liquid phase redistribution is referred to as sintering stress in powder compact technology (Chiang et al., 1997; German, 1996). Tensile sintering stress results from the thermodynamic tendency to minimize the energy of solid and liquid surfaces, potentially causing growth of larger pores with concurrent elimination of smaller ones. A heterogeneous distribution of the sintering process within the powder compact induces stress gradients that may lead to void growth and coalescence and to macroscopic fractures (German, 1996). Such tensile

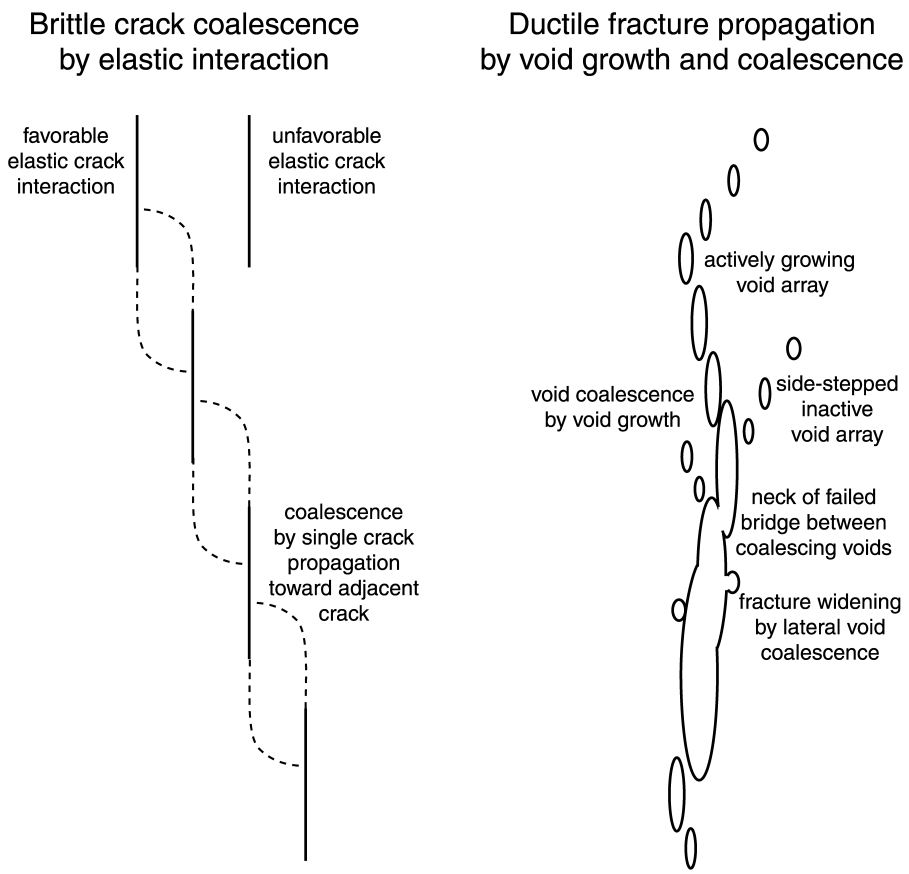

Fig. 13. Formation of en-échelon arrays by brittle and ductile fracture. Brittle fractures in en-échelon arrays coalesce by single-fracture propagation toward adjacent fractures. Elastic interaction favors a consistent stepping direction. Ductile fractures propagate by preferred void growth in en-échelon arrays and void coalescence. Switching between right- and left-stepping direction leads to zig-zag propagation paths.

sintering stress would be generated throughout the matrix causing distributed pore growth and coalescence away from the tips of already existing fractures.

Homogeneous sintering would result in an isotropic tensile sintering stress. A deviatoric component necessary for formation of elongate and crack-like pores may result from heterogeneous sintering or from superposition of an isotropic sintering stress with deviatoric external loading. Initial pore growth in clinker appears to be isometric suggesting that diffusive mass transfer associated with pore growth is efficient enough to maintain a thermodynamically more favorable spherical pore shape. An increasingly elongate pore shape with continued growth may reflect a feedback between enhanced mass transfer and tensile sintering stress. The overall decrease in aspect ratio from elongate pores to blunt-tipped fractures is likely to result from an increasing contribution of pore coalescence over single pore growth and an increasing preference in pore coalescence at fracture tips compared with coalescence along fracture sides with increasing fracture length.

4.4. Significance

The inferred high-temperature/low-pressure conditions during combustion alteration are outside typical crustal thermobaric gradients. Comparable conditions may be found, however, in contact of high-level radioactive waste deposits and during enhanced petroleum recovery by fire flooding in heavy crude oil reservoirs (Lore et al., 2002). Under these conditions, fractures similar to those observed in clinker may result in significant changes in the permeability structure and thus in fluid flow and heat transport.

In addition, we suggest that ductile opening-mode fractures in clinker illustrate the significance of inelastic deformation in controlling initiation, propagation, and shape of opening-mode rock fracture under a variety of subsurface conditions. We propose that significant inelastic deformation in the surrounding host rock concurrent with fracture opening is a defining characteristic of ductile rock fracture. Such inelastic deformation may result from diffusion and solution mass transfer, crystal-plasticity, grain-boundary sliding, and viscous flow of a melt phase. Based on the extent of mass transfer or crystal-plasticity involved in fracture opening and propagation we envision brittle mechanical fracture propagation and ductile fracture by void growth and coalescence as representing two end member types of rock fracture (Fig. 14). Localized mass transfer within the fracture process zone may lead to chemical bond weakening associated with subcritical

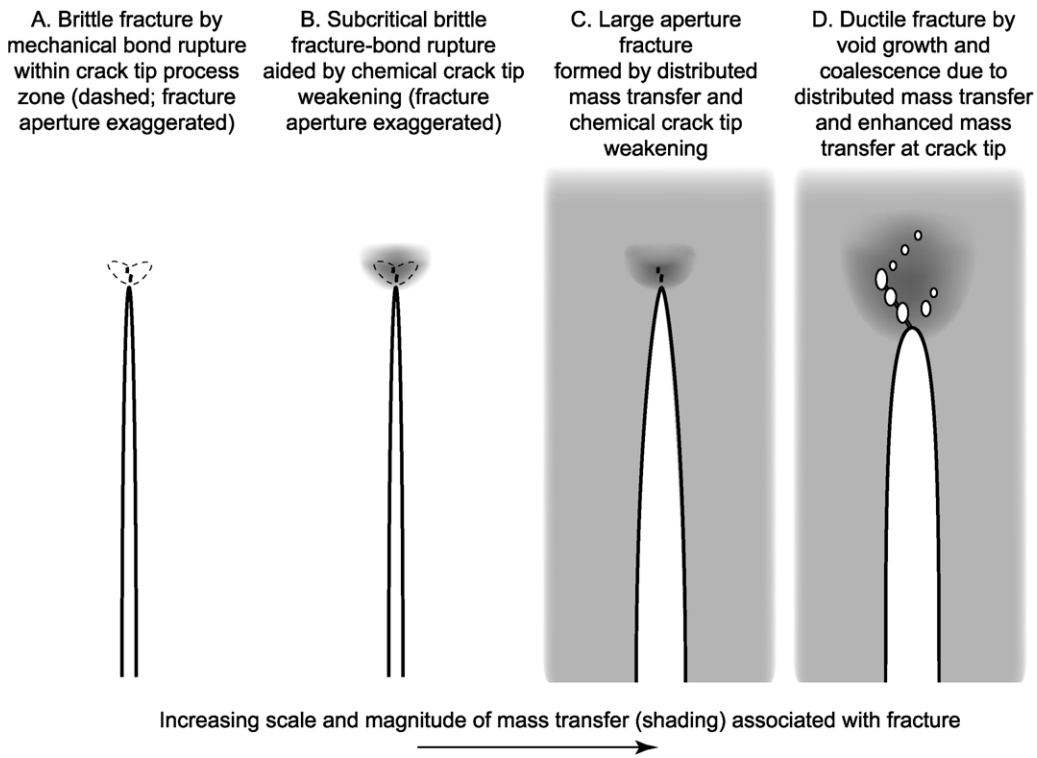

Fig. 14. Interaction of mass transfer with opening-mode fracture, arranged from no associated mass transfer (brittle failure) via subcritical fracture to significant mass transfer in the host rock and at the fracture tip allowing the formation of large-aperture and ductile fractures.

fracture propagation (B in Fig. 14). Distributed mass transfer within the host rock would accommodate fracture opening in excess of elastic fracture opening leading to large-aperture fractures (C in Fig. 14). Large-aperture fractures are usually observed as veins (Vermilye and Scholz, 1995; Gillespie et al., 2001), under upper-crustal conditions frequently in fine-grained rocks of reactive composition such as organic-rich mudstone and carbonate (Eichhubl and Behl, 1998). Isolated veins are typically filled with fracture cement of mineralogical, isotopic, and trace element composition reflecting that of the host rock (Dietrich et al., 1983; Eichhubl and Boles, 1998) indicative of a link between host rock mineral dissolution, fracture opening, and fracture cementation. Such a link would not only be consistent with consecutive stages of vein mineralization reflecting distinct diagenetic reactions during a burial trend but also with repeated cycles of fracture opening and sealing that correlate with distinct stages of burial diagenesis (Eichhubl and Boles, 1998). Whereas solution mass transfer would accommodate large-aperture fracture opening under upper-crustal conditions, crystal plasticity and partial melting may accompany the formation of veins in metamorphic rock and of melt segregation veins under mid- to lower-crustal conditions. Ductile fracture processes involving void nucleation and growth on a lithospheric scale have recently been proposed by Regenauer-Lieb (1999) to explain the localization of intraplate volcanism.

In addition to large-aperture opening-mode fractures, extensive inelastic deformation may accompany formation of faults resulting in displacement to length ratios that exceed those predicted for faults in perfectly brittle materials. The amount of finite fault displacement, the rate of slip accumulation, and the dynamics of fault slip, i.e. stick–slip versus stable sliding, may be controlled by the extent and type of inelastic deformation occurring in the adjacent host rock, thus potentially affecting the seismic behavior of crustal-scale faults.

5. Conclusions

Opening-mode fractures in clinker are characterized by: (1) high ratios of maximum fracture aperture over fracture length; (2) blunt fracture tips; (3) an increased abundance of elongate pores ahead of fracture tips and adjacent to larger fractures; and (4) zig-zag propagation paths. Fractures form during high-temperature/low pressure combustion alteration and partial melting of siliceous mudstone by a process of void growth and coalescence. Void growth and coalescence are inferred to result from solution mass transfer and possible bulk melt movement leading to the formation of elongate pores and macroscopic blunt-tipped fractures. A tensile sintering stress resulting from the tendency toward energy minimization of liquid and solid surfaces may cause the growth of elongate pores to macroscopic fractures and local rupture of bridges between pores.

Fracture growth associated with significant inelastic deformation of the host rock is considered characteristic of ductile fracture. Such inelastic deformation may lead to high

ratios of aperture over length for opening-mode fractures and of slip over fracture length for shearing-mode fractures and faults. It is suggested that processes of ductile fracture may be a significant process in metamorphic and magmatic systems as well as in reactive diagenetic environments.

Acknowledgements

This study was funded in part by DOE contract DE-PS22-94BC1114973, by the David and Lucile Packard Foundation, and by the Stanford Rock Fracture Project. Bob Jones is thanked for help with microprobe analyses. This study benefited from discussions with Bob McMeeking, UC Santa Barbara, and Reiner Dauskardt, Stanford University. David Pollard and JSG reviewer Susan Agar are thanked for detailed reviews and suggestions.

References

Anderson, T.L., 1995. Fracture Mechanics. Fundamentals and Applications, 2nd Edition, CRC Press, Boca Raton.

Arnold, R., Anderson, R., 1907. Geology and oil resources of the Santa Maria Oil District, Santa Barbara Co., CA. United States Geological Survey Bulletin 322, 48–52.

Atkinson, B.K., 1984. Subcritical crack growth in geological materials. Journal of Geophysical Research 89, 4077–4114.

Bentor, Y.K., Kastner, M., 1976. Combustion metamorphism in Southern California. Science 193, 486–488.

Bentor, Y.K., Kastner, M., Perlman, I., Yellin, Y., 1981. Combustion metamorphism of bituminous sediments and the formation of melts of granitic and sedimentary composition. Geochimica et Cosmochimica Acta 45, 2229–2255.

Bluhm, J.I., Morrissey, R.J., 1965. Fracture in a tensile specimen. In: Yokobori, T., Kawasaki, T., Swedlow, J.L. (Eds.), Proceedings of the First International Conference on Fracture, Sendai, Japan 3, pp. 1739–1780.

Chiang, Y.-M., Birnie, D. III, Kingery, W.D., 1997. Physical Ceramics, Wiley, New York.

Cisowski, S.M., Fuller, M., 1987. The generation of magnetic anomalies by combustion metamorphism of sedimentary rock, and its significance to hydrocarbon exploration. Geological Society of America Bulletin 99, 21–29.

Dalgleish, B.J., Johnson, S.M., Evans, A.G., 1984. High-temperature failure of polycrystalline alumina: I. Crack nucleation. Journal of the American Ceramic Society 67 (11), 741–750.

Dietrich, D., McKenzie, J.A., Song, H., 1983. Origin of calcite in syntectonic veins as determined from carbon–isotope ratios. Geology 11, 547–551.

Du, Y., Aydin, A., 1991. Interaction of multiple cracks and formation of echelon crack arrays. International Journal for Numerical and Analytical Methods in Geomechanics 15, 205–218.

Eichhubl, P., Behl, R.J., 1998. Diagenesis, deformation, and fluid flow in the Miocene Monterey Formation. In: Eichhubl. P. (Ed.), Diagenesis, Deformation, and Fluid Flow in the Miocene Monterey Formation of Coastal California. SEPM Pacific Section Special Publication 83, pp. 5–13.

Eichhubl, P., Boles, J.R., 1998. Vein formation in relation to burial diagenesis in the Miocene Monterey Formation, Arroyo Burro Beach, Santa Barbara, California. In: Eichhubl. P. (Ed.), Diagenesis, Deformation, and Fluid Flow in the Miocene Monterey Formation of Coastal California. SEPM Pacific Section Special Publication 83, pp. 15–36.

Eichhubl, P., Aydin, A., Lore, J., 2001. Opening-mode fracture in siliceous mudstone at high homologous temperature—effect of surface forces. Geophysical Research Letters 28, 1299–1302.

Engelder, T., Fischer, M., Gross, M.R., 1993. A Short Course Manual on Geological Aspects of Fracture Mechanics, Geological Society of America, Boston.

Evans, A.G., Blumenthal, W., 1984. High temperature failure mechanisms in ceramic polycrystals. In: Tressler, R.E., Bradt, R.C. (Eds.), Deformation of Ceramic Materials II, Plenum Press, New York, pp. 487–505.

German, R.M., 1996. Sintering Theory and Practice, Wiley, New York.

Gillespie, P.A., Walsh, J.J., Watterson, J., Bonson, C.G., Manzocchi, T., 2001. Scaling relationships of joint and vein arrays from The Burren, Co. Clare, Ireland. Journal of Structural Geology 23, 183–201.

Hill, R., 1950. The Mathematical Theory of Plasticity, Oxford Science Publications, Oxford.

Ingraffea, A.R., 1987. Theory of crack initiation and propagation in rock. In: Atkinson, B.K., (Ed.), Fracture Mechanics of Rock, Academic Press, London, pp. 71–110.

Jin, Q., Wilkinson, D.S., Weatherly, G.C., 1999. The contribution of viscous flow to creep deformation of silicon nitride. Materials Science and Engineering A271, 257–265.

Johannes, W., 1989. Melting of plagioclase–quartz assemblages at 2 kbar water pressure. Contributions to Mineralogy and Petrology 103, 270–276.

Johnson, D.M., Hooper, P.R., Conrey, R.M., 1999. XRF analysis of rocks and minerals for major and trace elements on a single low dilution li-tetraborate fused bead. Advances in X-ray Analysis 41, 843–867.

Keller, M.A., Isaacs, C.M., 1985. An evaluation of temperature scales for silica diagenesis in diatomaceous sequences including a new approach based on the Miocene Monterey Formation, California. Geo-Marine Letters 5 (1), 31–35.

Kinloch, A.J., Young, R.J., 1983. Fracture Behaviour of Polymers, Applied Science Publishers, London.

Lore, J., Eichhubl, P., Aydin, A., 2002. In-situ combustion of hydrocarbons and its impact on alteration and fracturing of siliceous mudstone, Orcutt Field, California. Journal of Petroleum Science and Engineering.

Nicholson, R., Pollard, D.D., 1985. Dilation and linkage of échelon cracks. Journal of Structural Geology 7, 583–590.

Olson, J., Pollard, D.D., 1991. The initiation and growth of en échelon veins. Journal of Structural Geology 13, 595–608.

Peck, L., Barton, C.C., Gordon, R.B., 1985. Microstructure and the resistance of rock to tensile fracture. Journal of Geophysical Research 90, 11,533–11,546.

Pollard, D.D., Aydin, A., 1988. Progress in understanding jointing over the past century. Geological Society America Bulletin 100, 1181–1204.

Pollard, D.D., Segall, P., 1987. Theoretical displacements and stresses near fractures in rock: with applications to faults, joints, veins, dikes, and solution surfaces. In: Atkinson, B.K., (Ed.), Fracture Mechanics of Rock, Academic Press, London, pp. 277–349.

Regenauer-Lieb, K., 1999. Dilatant plasticity applied to Alpine collision: ductile void growth in the intraplate area beneath the Eifel volcanic field. Journal of Geodynamics 27, 1–21.

Thomason, P.F., 1990. Ductile Fracture of Metals, Pergamon Press, Oxford.

Vermilye, J.M., Scholz, C.H., 1995. Relation between vein length and aperture. Journal of Structural Geology 17, 423–434.

Whittaker, B.N., Singh, R.N., Sun, G., 1992. Rock Fracture Mechanics. Principles, Design, and Applications, Elsevier, Amsterdam.

Wiederhorn, S.M., Hockey, B.J., French, J.D., 1999. Mechanisms of deformation of siliceous nitride and silicon carbide at high temperatures. Journal of the European Ceramic Society 19, 2273–2284.

Wilkinson, D.S., Caceres, C.H., Robertson, A.G., 1991. Damage and fracture mechanisms during high-temperature creep in hot-pressed alumina. Journal of the American Ceramic Society 74, 922–933.